100-Gb/s/λ PAM-4 EAM-integrated DBR-LD Supporting Multiple Sub-Channels within 1.29 μm window

Oh Kee Kwon, Chul Wook Lee, Su Ik Park, Kyoung Su Park, and Ki Soo Kim

Abstract—We present a distributed Bragg reflector-laser diode (DBR-LD) monolithically integrated with an electroabsorption modulator (EAM) offering a 100-Gb/s pulse amplitude modulation 4-level (PAM-4) signal per sub-channel under a CWDM window of 1.29 μm. For the integrated structure, the DBR-LD and EAM were implemented using a trenched waveguide in the tuning sections for achieving energy-efficient wavelength-tuning and a deep ridge waveguide with an optimized structure for a 100-Gb/s PAM-4 operation, respectively. The fabricated chip shows a threshold current of approximately 12 mA and a tuning range of greater than 13 nm, which corresponds to a wavelength band capable of supporting 16 channels with a 150-GHz grid, while maintaining a side mode suppression ratio of greater than 40 dB. In dynamic tests, the results show clear 100-Gb/s PAM-4 eye openings with an outer extinction ratio of more than 4 dB and a transmitter dispersion eye closure quaternary of less than 1.5 dB for all measured channels.

Index Terms— Wavelength division multiplexing, semiconductor lasers, distributed Bragg reflector lasers, laser tuning, electroabsorption, pulse amplitude modulation.

I. Introduction

WAVELENGTH-tunable lasers continue to have a significant impact on diverse fields of science and technology and are needed for numerous applications, including spectroscopy, medicine, gas-detection, precise measurements, frequency modulated continuous wave lidar, and optical communication. In particular, a tunable optical transmitter operating at a data rate of dozens of gigabits per second or higher for each channel in a wavelength division multiplexing (WDM) system is one of the essential components of next-generation wavelength-agile access networks, realizing effectively employing wavelength resources, dynamic channel allocation, and flexible networks as well as a reduction in the inventory cost when utilized as a replacement for wavelength-fixed sources [1–3].

A distributed Bragg reflector-laser diode (DBR-LD) with a single grating mirror is the most suitable candidate for such networks owing to its compactness, simple structure, and easy wavelength calibration compared with DBR structures having two different grating mirrors [4–6]. In addition, by introducing two different tuning methods simultaneously, its tuning range has been considerably increased to up to 30 nm for the C-band [7, 8], and by applying heater tuning only, is greater than 15 nm for the O-band [9].

We recently developed an electroabsorption modulator (EAM)-integrated DBR-LD supporting a 25-Gb/s non-return-to-zero signal for each channel [8, 10]. Based on this result, we believe an EAM-integrated DBR-LD can be effectively used as a cost-effective light source enabling common public ratio interface (CPRI) line bit rate option 10 (i.e., 24.33024 Gb/s) in a mobile front-haul network (MFH) based on multichannel CWDM applications with a multi-sub-channel optical interface [11].

By contrast, to enhance the transmission capacity under the given bandwidth, modulation formats with a higher spectral efficiency, similar to pulse amplitude modulation 4-level and 8-level (PAM-4 and -8) [12-15], are required. We have developed an EAM-integrated DBR-LD capable of generating a 100-Gb/s PAM-4 signal for each wavelength and having 16 channels with a 150-GHz grid by modifying the band gaps of the epitaxial layers for 1.29-μm operation, reducing the capacitances of the EAM and utilizing the RF resonance for a larger modulation bandwidth, and introducing a novel heat-confining structure for

Manuscript received January 26, 2023; revised; March 12, 2023; Published; xx. Xx, 2023. Date of publication xx xx, 2023; data of current version xx xx, 20xx.This work was supported by ICT R&D programs of MSIP/IITP, South Korea [No. 2020-0-00847, 2022-0-00584] and ETRI Grant, South Korea [No. 22YB1710].

Oh Kee Kwon is with Photonic/Wireless Devices Research Division, Terrestrial & Non-Terrestrial Integrated Telecommunications Research Lab., ETRI, Daejeon 305-350, South Korea (e-mail: okkwon@etri.re.kr).

Chul Wook Lee is Photonic/Wireless Devices Research Division, Terrestrial & Non-Terrestrial Integrated Telecommunications Research Lab., ETRI, Daejeon 305-350, South Korea (e-mail: leecw@etri.re.kr)

Su Ik Park is with Essence Photonics Inc. #302-2, 218, Gajeong-ro, Yuseong-gu, Daejeon, South Korea and Department of Photonics and Nanoelectronics, Hanyang University ERICA, Gyeonggi, South Korea (leo.park@essencephotonics.com).

Kyoung Su Park is with Opticore Inc., #501, The First Tower 3, 602, Dongtangiheung-ro, Hwaseong, Gyeonggi, South Korea and Department of Electronics Engineering, Kangwon National University, 1 Gangwondaehakgil, Chuncheon, South Korea (kspark@opticore.co.kr).

Ki Soo Kim is Photonic/Wireless Devices Research Division, , Terrestrial & Non-Terrestrial Integrated Telecommunications Research Lab., ETRI, Daejeon 305-350, South Korea (e-mail: kimks1136@etri.re.kr).

a higher tuning efficiency, building on our previous structure [10].

In this paper, we report the fabricated LD and its operational properties. The rest of this paper is organized as follows. The device structure and its fabrication are described in Section 2. Section 3 presents the experimental results for the LD chip and its module. Finally, Section 4 summarizes the results of this study.

II. Device Structure and Fabrication

An image of a fabricated chip and the epitaxial layer structure of the EAM-integrated DBR-LD are shown in Figs. 1(a) and 1(b), respectively. The LD is composed of gain, phase control (PC), DBR, EAM, and spot-size converter (SSC) sections. The length of each of these sections was designed to be 350, 120, 230, 165, and 250 μm, respectively. For this structure, the output light is emitted from the anti-reflection (AR) coated facet of the SSC and is intensity-modulated by the voltage V_{EAM} though the metallic pad of the EAM section. The operating wavelength is selected based on the lasing condition of the DBR-LD, the cavity of which is from the DBR to the gain section, and the wavelength is both coarsely and finely tuned using the voltages V_{DBR} and V_{PC} through a metal thin-film heater formed on top of the waveguide in the DBR and PC sections, respectively.

For the device, an active region within the gain section was designed for lasing near a wavelength of 1.29 μm. In addition, the epitaxial layer and waveguide in the EAM section were optimized for operation at a rate of 100-Gb/s PAM-4, and a heat-insulated structure in the tuning sections (i.e., DBR and PC) was applied to enhance the wavelength tuning efficiency [19]. First, to allow the LD to operate within a CWDM window of 1.29 μm, the Bragg wavelength and coupling coefficient of the grating were designed to be approximately 1.283 μm and 25 cm^{-1}, respectively. Specifically, a 200-μm-long grating layer has a 25-nm thick InGaAsP material with a bandgap wavelength of approximately 1.2 μm. For this structure, a power reflectivity of approximately 0.25 was obtained.

The active region, which contains multiple quantum wells (MQWs) and separate confinement heterostructure (SCH) layers in the gain section, was designed to create a gain near a wavelength of 1.29 μm, whereas those of the EAM were designed to have a detuning of approximately 50 nm from the gain-peak wavelength and to obtain a higher extinction and larger bandwidth. Details of the layer structures of each section are listed in Table 1. After the growth of the epitaxial layers, photo-luminescent (PL) tests were conducted on the grown layer of each section. The peak wavelengths in the gain, EAM, and passive core sections obtained were approximately 1.29, 1.24, and 1.15 μm, respectively.

After the PL test, the active region and core layer in the tuning sections and the SSC were etched to widths of approximately 1.2, 1.2, and 0.6 μm, respectively. For the waveguide structure of the device, the DBR-LD and SSC were fabricated into an etched-mesa buried hetero-structure (EMBH) [7, 20] with a width of 12, 9, 8 μm for the gain and tuning sections and the SSC, respectively, and the EAM was made into

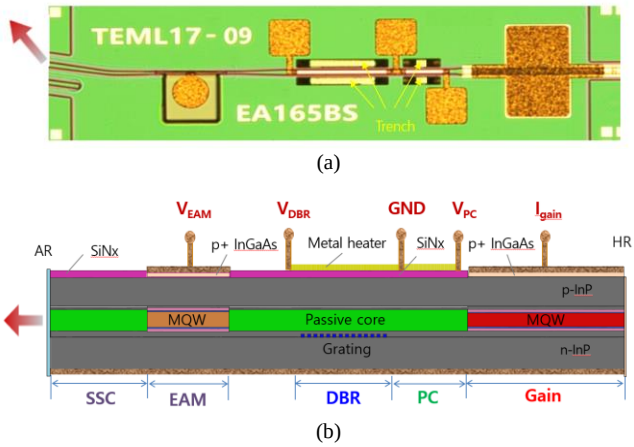

Fig. 1. (a) Chip (top-view) and (b) layer structure (side-view) of the EAM-integrated DBR-LD. The SSC is introduced to improve an alignment tolerance with an optical fiber, and the output waveguide is tilted 9° to reduce the residual optical feedback from the output facet [15–17].

TABLE I
Epitaxial Layers of Gain, Passive, and EAM Sections

Section	Structure	InGaAsP material Thickness, bandgap wavelength, strain
gain	7 QWs	
(active)	Well	6 nm, 1.38 μm, compressive 0.8%
	Barrier	8 nm, 1.1 μm, tensile 0.6%
	Inner SCH	35 nm, 1.08 μm, lattice-matched
	Outer SCH	45 nm, 1.05 μm, lattice-matched
Passive core	Bulk	0.27 μm, 1.15 μm, lattice-matched
EAM	12 QWs	
	Well	8.5 nm, 1.28 μm, compressive 0.5%
	Barrier	6 nm, 1.1 μm, compressive 0.4%
	SCH	70 nm, 1.15 μm, lattice-matched

a deep ridge waveguide (DRWG) with a width of approximately 2.2 μm. A 3D beam propagation method (BPM) simulation was conducted to analyze the beam propagation properties of the SSC, as shown in Fig. 2. In this simulation, the waveguide mode of the EAM was utilized as an input (i.e., Z= 0 μm). We confirmed that the full width at half maximum (FWHM) of the far-field pattern (FFP) was converted into 14.5° × 16.8° at Z= 300 μm.

After the formation of the waveguide, a benzo-cyclobutene (BCB) island for reducing the parasitic capacitance was closely implemented using the waveguide of the EAM section. A Ti/Pt/Au metal was then formed as a p-type contact of the gain and EAM sections, and a Cr/Au-based thin-film metal was used as the metal heater of the tuning sections. Compared with the previous structure [10], to improve the electrical isolation between the gain and PC sections and to simplify the fabrication

process, the tuning operation of the PC section for fine tuning was changed from plasma into heater tuning.

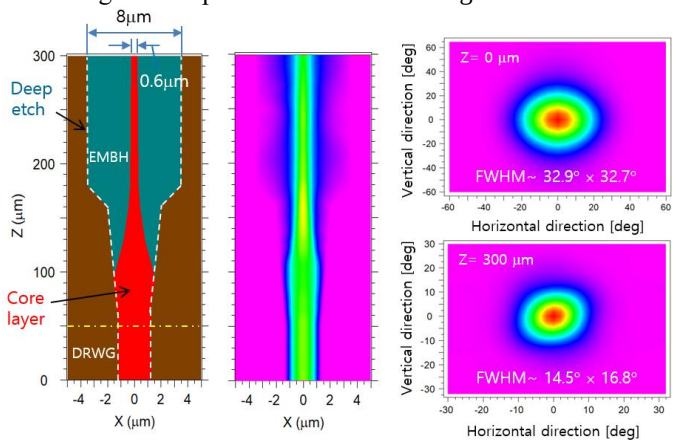

(a) (b) (c)

Fig. 2. (a) Schematic view of the SSC with a 0.6 μm-wide core layer and an 8 μm-wide EMBH, (b) 3D BPM simulation result, and (c) FFPs at Z = 0 μm (upper) and Z = 300 μm (lower).

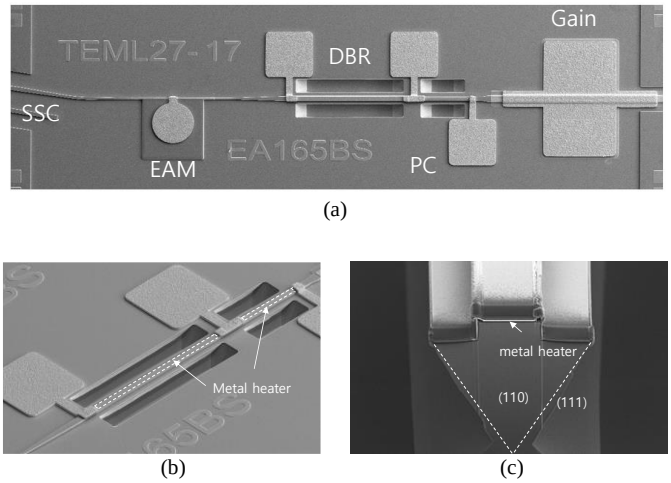

(a)

(b) (c)

Fig. 3. SEM images of (a) fabricated LD chip, (b) waveguide of the tuning sections with metal heaters, and (c) cross-sectional view of the DBR section.

For the wavelength tuning, a trenched waveguide structure that can effectively confine the heat created from the metal heater was introduced to achieve an energy-efficient tuning operation and was simply fabricated by forming a reverse-mesa (RM) shape without the use of a sacrificial layer. This RM structure was implemented using a SiNx etching mask below the EMBH by applying a Br-based InP selective wet etchant [21]. We confirmed experimentally that the lateral and vertical etch rates of the etchant were approximately 0.65 and 1.5 μm/min, respectively.

Figures 3(a)–3(c) show scanning electron microscope (SEM) images of the fabricated chip, the waveguide of the tuning sections, and a cross-sectional view of the DBR section, respectively. After the following fabrication processes, including lapping, n-type metallization, chip-bar scribing, and facet coatings, the static properties were tested. In addition, after scribing, the chip was then bonded onto a sub-mount with electrical lines for light generation (I_{gain}), tuning (V_{PC} and V_{DBR}), modulation (V_{EAM}), and a 50-Ω load, as shown in Fig. 4.

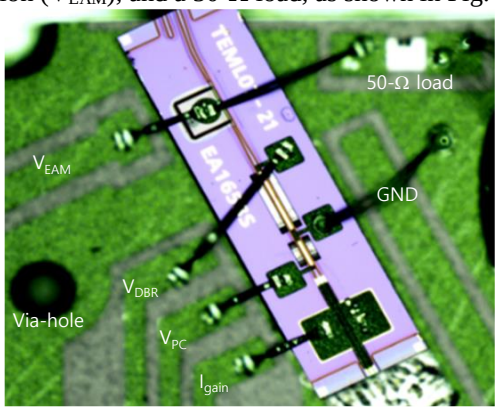

Fig. 4. Photograph of an EAM DBR-LD chip integrated onto a sub-mount with electrical lines and a 50-Ω load.

III. Results and Discussion

Figures 5(a) and 5(b) show typical light versus gain current (L-I_{gain}) characteristics and the output spectrum of the fabricated LD, respectively. Overall, excluding the results of the FFPs and operating wavelength, the lasing properties were nearly the same as those of the previous structure [10]. Specifically, the threshold current and slope efficiency appeared to be approximately 12 mA and 0.18 W/A, respectively and the peak wavelength λ_{peak} and side mode suppression ratio (SMSR) were approximately 1283 nm and greater than 40 dB, respectively. The FFPs of the fabricated LD chip were measured in this experiment, as illustrated in Fig. 6. By applying Gaussian fitting, we obtained a FWHM of 14.9° and 16.4° for the horizontal and vertical directions, respectively. These results match well with the values obtained from the BPM simulation.

To check the tuning operation, the peak wavelength λ_{peak} and the SMSR were measured as a function of the voltage of the DBR section, V_{DBR}, as shown in Fig. 7. With an increase in V_{DBR}, λ_{peak} is shifted to a longer wavelength owing to the change in the heat-induced refractive index, and the tuning range has a parabolic shape with some mode jumps, the interval of which corresponds to the free spectral range (FSR) of the cavity. By adjusting the PC voltage V_{pc}, λ_{peak} can be continuously changed within the FSR, allowing for precise positioning of the operating wavelength at any assigned channel wavelength within the tuning range by using a combination of V_{DBR} and V_{PC}. To achieve effective wavelength control, it is recommended to perform rough tuning with V_{DBR} first, followed by fine tuning with V_{PC}. The tuning range appears to be approximately 17 nm (i.e., 1283 – 1300 nm) within a V_{DBR} of 1.5 V, which satisfies the sub-channel window of 1.29 μm in the MFH (i.e., 1284.2 – 1296.1 nm) [11].

To examine the operational properties of the EAM, the chip was packaged on the sub-mount and tested in a module form. For the extinction and modulation property of the EAM-integrated LD under a given MQW structure of the EAM, it is

extremely important to select a proper EAM length L_{EAM} to simultaneously satisfy the data rate and extinction. This is because the modulation bandwidth and optical absorption are significantly dependent on L_{EAM} according to the junction capacitance model [22] and the optical power transmission model [23, 24], respectively. After testing the electro-optic (EO) response and output power variation with respect to the EAM voltage V_{EAM} for the modules, we confirmed that they have a −3-dB bandwidth of more than 38 GHz for all channels, as shown in Fig. 8, which is necessary for a 100-Gb/s PAM-4 operation, and a static ER of −5 dB at a V_{EAM} of −2.0 V for an L_{EAM} of 165 μm. The increase in modulation bandwidth in this structure can be attributed to the reduction in capacitances, which is achieved through a decrease in EAM length, an increase in intrinsic layer thickness (by increasing the QW number), the effective use of low dielectric materials like BCB. Additionally, the RF resonance via wire boning can also contribute to the increased bandwidth [22].

The extinction ratio (ER), the value normalized by the power obtained at zero voltage, was measured for all channels. Figure 9 shows the ER curve for ch 1 (1284.22 nm), ch 7 (1288.94 nm), and ch 16 (1296.04 nm). It appears that the ER has a reverse sigmoid shape and slowly falls off with an increase in the number of channels. We believe that the degradation of the ER with the number of channels is mainly due to the increase in the detuning between the absorption peak wavelength and the operating wavelength, as well as a weakening of the stark quantum-confined effect, similar to inhomogeneous broadening [25, 26]. Consequently, an ER of –

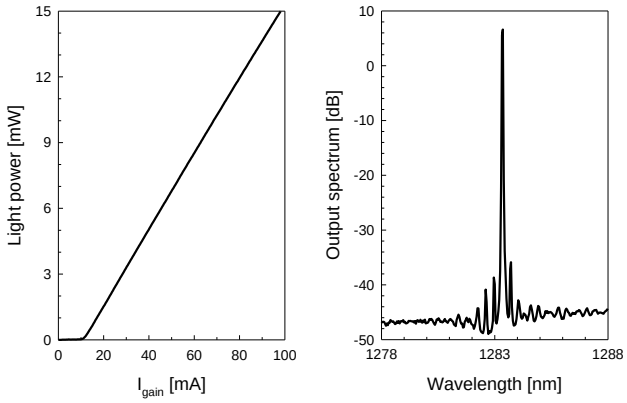

(a) (b)

Fig. 5. (a) L-I_{gain} characteristics and (b) output spectrum of the fabricated LD chip. In (b), the spectrum was obtained at a gain current I_{gain} of 100 mA and its fiber coupled power was approximately 5mW.

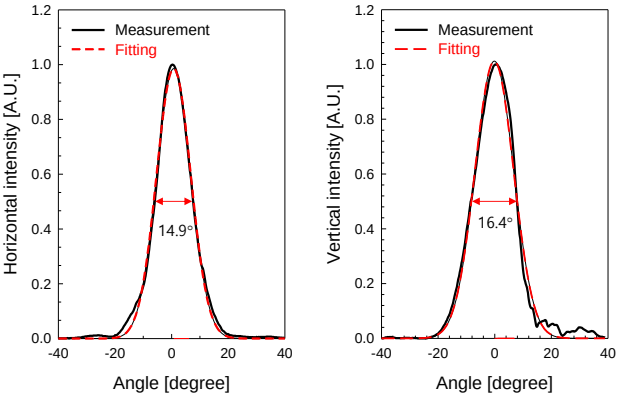

(a) (b)

Fig. 6. (a) Horizontal and (b) vertical intensity patterns with respect to the angle. Black solid and red dashed lines denote the measured and fitted values, respectively.

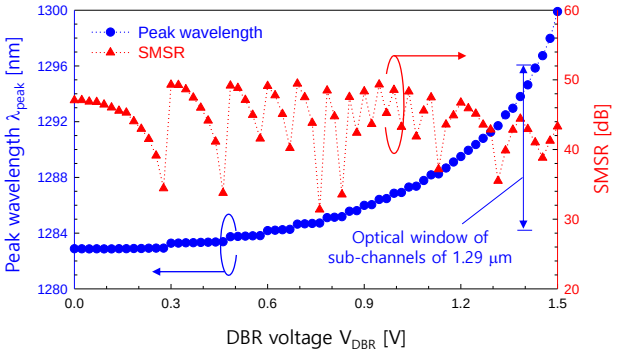

Fig. 7. Peak wavelength λ_{peak} (blue, circle) and SMSR (red, triangle) characteristics of the fabricated LD chip with respect to the voltage V_{DBR}.

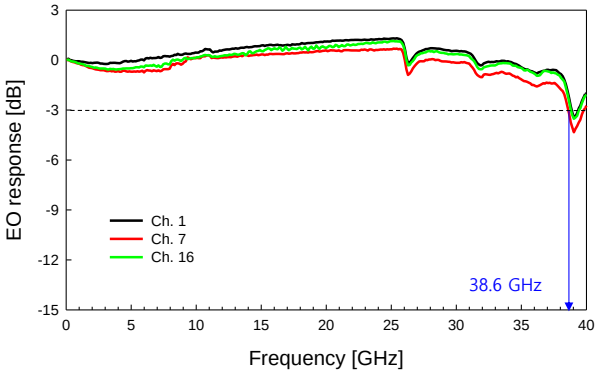

Fig. 8. EO responses of the EAM-integrated DBR-LD for channel 1, 7, and 16. The EAM voltage V_{EAM} was set to −2 V during the measurement, and the −1dB bandwidth of the photodiode was approximately 40 GHz. Please note that the measured data has not been de-embedded.

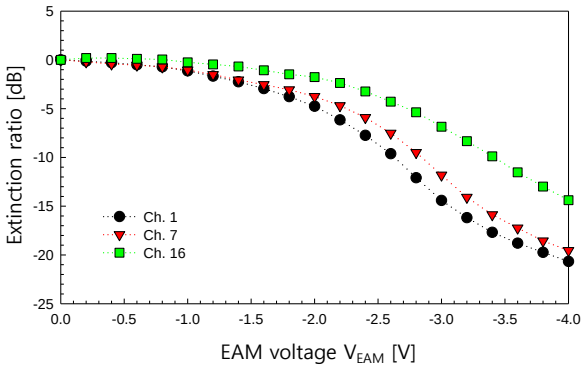

Fig. 9. Extinction ratios of the module with respect to the EAM voltage V_{EAM} for channel 1, 7, and 16.

5 dB is obtained at approximately –2.2 and –2.7 V for ch 7 and ch 16, respectively.

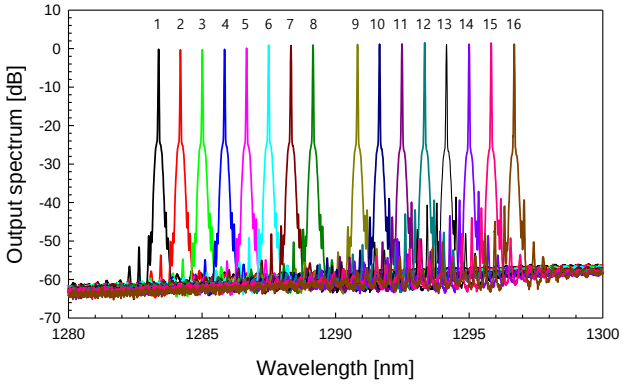

Fig. 10. Superimposed tuning spectra of 16 channels under 100-Gb/s PAM-4 operation. The channel grid is 150 GHz.

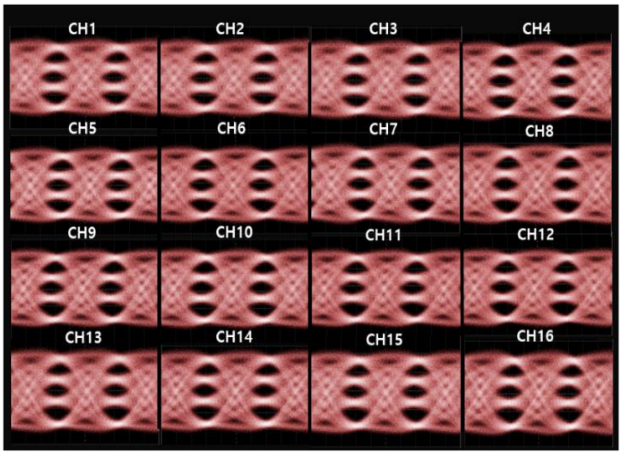

Fig. 11. Measured 100-Gb/s PAM-4 eye patterns for 16 channels. The receiving filter bandwidth of 37.3 GHz was used.

A large-signal modulation test was conducted for the 100-Gb/s PAM-4 signal. During the test, an electrical 100-Gb/s PAM-4 signal with a pseudorandom binary sequence pattern of 2^{15}-1 was generated using a pulse pattern generator (Anritsu MU196020A), and amplified by a broad band amplifier (with an S21 bandwidth of 56 GHz). Each DC current or voltage was supplied to the module pad through a single-tip probe, and the EAM bias voltage V_{bias} and PAM-4 signal were combined through a bias-tee and applied to the EAM pad through a bonding wire from a GSG line placed on the module. During this test, the peak-to-peak voltage V_{pp} was set to 2 V, and the bias voltage was adjusted with an increase in the number of channels to allow the EAM to operate within a linear region along the ER curve.

Figure 10 shows superimposed output spectra of the 16 channels. The gain current I_{gain} was fixed to 100 mA, and each spectrum was obtained with a simultaneous control of the heater voltages of the DBR and PC sections, which can allow 16 channels to be aligned within an interval of 150 GHz (which corresponds to approximately 0.79 nm at a wavelength of 1.29 μm). The spectra show a nearly uniform power and a good dynamic single mode across the channel under modulation.

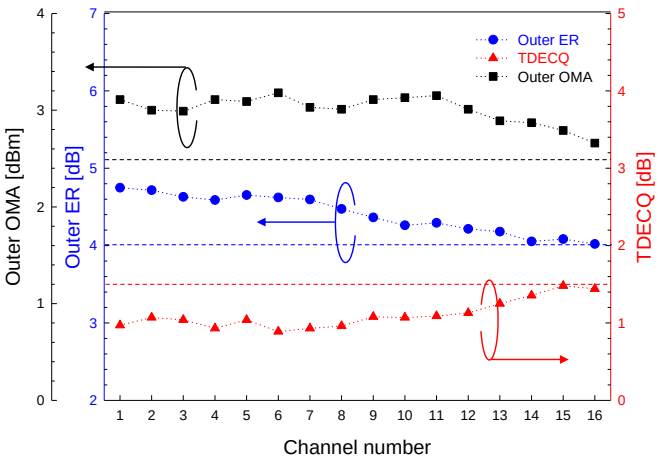

Fig. 12. Outer ER (blue, circle), TDECQ (red, triangle), and outer OMA (black, square) of 100-Gb/s PAM-4 eye patterns with respect to the number of channels.

Specifically, a peak power difference of less than 1 dB and an SMSR of more than 40 dB were obtained within a wavelength range of approximately 15 nm.

An optical signal from the module was directly received by a digital communication analyzer (Keysight N1030A). Figure 11 shows the measured optical eye patterns for the 100-Gb/s PAM-4 signals. Clear eye openings are shown for all 16 channels. An outer ER of more than 4 dB, a transmitter dispersion eye closure quaternary (TDECQ) of less than 1.5 dB, and outer OMA (optical modulation amplitude) of greater than 2.5 dBm for each channel were obtained, as shown in Fig. 12. Regarding the effect of the wavelength tuning on the signal quality, the PAM-4 signal was highly sensitive to V_{bias} and V_{pp} owing to the limited linearity of the ER curve. Specifically, when the number of channels increases under a certain optimal bias condition, the ER is decreased with a variation of less than 1 dB, the TDECQ is increased with a deviation of less than 0.5 dB, and the OMA is changed with a variation of less than 0.5 dBm over the range of 1284.2–1296.1 nm.

IV. Summary

We developed a 100-Gb/s PAM-4 EAM-integrated DBR-LD that can provide multiple sub-channels within a CWDM window of 1.29 μm. The band gaps of the epitaxial layers in the gain section were adjusted for 1.29-μm operation. In addition, the epitaxial layer and waveguide structures in the EAM section were optimized for 100-Gb/s PAM-4 operation, and the RM structure in the tuning sections was implemented for energy-efficient tuning. Using the fabricated LD, through simultaneous control of the tuning voltages, we obtained 16 channels spaced within a wavelength grid of 150 GHz (i.e., 1284.2–1296.1 nm) with an SMSR of greater than 40 dB. Using a module with a 165-μm long EAM-integrated DBR-LD, clear 100-Gb/s PAM-4 eye openings with an outer ER of >4 dB and a TDECQ of <1.5 dB were achieved for all operating channels. From these results, we can conclude that the EAM-integrated DBR-LD can

be used as an effective light source for next-generation MFH networks.

REFERENCES.

[1] J. Shin, S. Hong, J. Y. Lim, S. Cho, H. Y. Rhy, and G. Y. Yi, "CWDM network with dual sub-channel interface for mobile fronthaul and backhaul deployment," in *Proc. 16th Int. Conf. Adv. Commun. Technol.*, Feb. 2014, pp. 1009–1102.

[2] J. Zhu, A. Wonfor, S. H. Lee, S. Pachnicke, M. Lawin, R. V. Penty, J.-P. Elbers, R. Cush, M. J. Wale, and I. H. White, "Athermal colorless C-band optical transmitter system for passive optical networks," *J. Lightw. Technol.*, vol. 32, no. 22, pp. 4253-4260, Nov. 2014.

[3] I. A. Alimi, A. L. Teixeira, and P. P. Monterio, "Toward an efficient C-RAN optical fronthaul for the future networks: a tutorial on technologies requirements, challenges, and solutions," *IEEE Comm. Surveys & Tutorials*, vol. 20, no. 1, pp. 708-769, First Quarter 2018.

[4] J. S. Barton, E. J. Skogen, M. L. Masanovic, S. P. DenBaars, and L.A. Coldren, **"**A widely tunable high-speed transmitter using an integrated SGDBR laser-semiconductor optical amplifier and Mach-Zehnder modulator," *IEEE J. Sel. Top. Quantum Electron*. vol. 9, no. 5, pp. 1113-1117, Sep./Oct. 2003.

[5] A. J. Ward, D. J. Robbins, G. Busico, E. Barton, L. Ponnampalam, J. P. Duck, N. D. Whitbread, P. Williams, D. C. J. Reid, A. C. Carter, and M. J.Wale, "Widely tunable DS-DBR laser with monolithically integrated SOA: Design and performance," *IEEE J. Sel. Top. Quantum Electron*., vol. 11, no. 1, pp. 149–156, Jan./Feb. 2005.

[6] T. Shindo, N. Fujiwara, Y. Ohiso, T. Sato, H. Matsuzaki, "Quasi-continuous tuning of a 1.3-μm-wavelength superstructure grating distributed Bragg reflector laser by enhancing carrier-induced refractive index change," *Opt. Exp*., vol. 29, no. 1, pp. 232-243, Jan. 2021.

[7] O. K. Kwon, C. W. Lee, K. S. Kim, S. H. Oh, and Y. A. Leem, "Proposal of novel structure for wide wavelength tunable in distributed Bragg reflector laser diode with single grating mirror," *Opt. Exp*., vol. 26, no. 22, pp. 28704-28712, Oct. 2018.

[8] O. K. Kwon, C. W. Lee, and K. S. Kim, "Electroabsorption modulator-integrated distributed Bragg reflector laser diode for C-band WDM-based networks," *ETRI J.*, vol. 45, no.1, pp. 163-170, Feb. 2023.

[9] S. H. Oh, O. K. Kwon, K. S. Kim, and C. W. Lee, "1.3-μm and 10-Gb/s tunable DBR-LD for low-cost application of WDM-based mobile front haul networks," *Opt. Exp.*, vol. 27, no. 20, pp. 29241- 29247, Sept. 2019.

[10] O. K. Kwon, C. W. Lee, S. H. Oh, and K. S. Kim, "16-channel tunable and 25-Gb/s EAM-integrated DBR-LD for WDM-based mobile front-haul networks," *Opt. Exp.*, vol. 29, no. 2, pp. 1805-1812, Jan. 2021.

[11] TTA Standard for Multichannel CWDM Applications with Multi Sub-channel Optical Interface, *TTAE.KO-03.0022/R2*, 2018.

[12] N. Eiselt, J. Wei, H. Griesser, A. Dochhan, M. H. Eiselt, J. Elbers, J. J. V. Olmos, and I. T. Monroy, "Evaluation of Real-Time 8×56.25 Gb/s (400G) PAM-4 for Inter-Data Center Application Over 80 km of SSMF at 1550 nm," *J. Lightw. Technol.*, vol. 35, no. 4, pp. 955-962, Feb. 2017.

[13] J. H. Lee, S. H. Chang, J. Y. Huh, S. K. Kang, K. Kim, and J. K. Lee, "EML based real-time 112Gbit/s (2 × 56.25 Gbit/s) PAM-4 signal transmission in C-band over 80 km SSMF for inter DCI applications," *Opt. Fiber Technol.*, vol. 45, pp. 141-145, July 2018.

[14] N. -P. Diamantopoulos, N. –P. Diamantopoulos, W. Kobayashi, H. Nishi, K. Takeda, "Amplifierless PAM-4/PAM-8 transmissions in O-band using a directly modulated laser for optical data-center interconnects," *Opt. Lett*. vol. 44, no. 1, pp. 9-12, Jan. 2019.

[15] Y.-H. Lin, H.-S. Lin, W.-L. Wu, C.-T. Tsai, C.-H. Cheng, T.-T. Shih, and G.-R. Lin, "100-Gbit/s/λ EML Transmitter and PIN-PD+TIA Receiver-Based Inter-Data Center Link," *J. Lightw. Technol.*, vol. 38, no. 8, pp. 2144-2151, April 2022.

[16] J. S. Choe, Y. H. Kwon, J. S. Sim, and S. B. Kim, "40 Gbps electroabsorption modulated DFB laser with tilted facet formed by dry etching," *Semicond. Sci. Technol*., vol. 22, no. 7, pp. 802–805, June 2007.

[17] O. K. Kwon, Y. S. Baek, and Yun C. Chung, "Electroabsorption modulated laser with high immunity to residual facet reflection," *IEEE J. Quantum Electron*., vol. 48, no. 9, pp. 1203-1213, Sept. 2012.

[18] Y. T, Han, O. K. Kwon, D. H. Lee, C. W. Lee, Y. A. Leem, J. U. Shin, S. H. Park, and Y. S. Baek, "A cost-effective 25-Gb/s EML TOSA using all-in-one FPCB wiring and metal optical bench," *Opt. Exp*., vol. 21, no. 22, pp. 26962-26971, Nov. 2013.

[19] S. I. Park, J. H. Jin, C. W. Lee, K. S. Kim, O. K. Kwon, K. S. Park, and J. I. Shim, "Heater-tuned DBR laser diode for high thermal efficiency," in *Proc. 28th Int. Semicond. Laser Conf. paper*, Oct. 2022, pp. TuP-31.

[20] O. K. Kwon, C. W. Lee, Y. A. Leem, K. S. Kim, S. H. Oh, and E. S. Nam, "1.5-μm and 10-Gbs^{-1} etched mesa buried heterostructure DFB-LD for datacenter networks, *Semicond. Sci. Technol.*, vol. 30, no. 10, pp. 105010-7, Oct. 2015.

[21] M. Aoki, M. Komori, T. Tsuchiya, H. Sato, K. Nakahara, and K. Uomi, "InP-based reverse-mesa ridge-waveguide structure for high-performance long-haul wavelength laser diodes," *IEEE J. Sel. Top. Quantum Electron*. vol. 3, no. 2, pp 672-683, April, 1997.

[22] O. K. Kwon, Y. T. Han, Y. S. Baek, and Y. C. Chung, "Improvement of modulation bandwidth in electroabsorption-modulated laser by utilizing the resonance property in bonding wire," *Opt. Exp.*, vol. 20, no. 11, pp. 11806-11812, May. 2012.

[23] J. Shim, B. Liu, and J. E. Bowers, "Dependence of transmission curves on input optical power in an electroabsorption modulator," *IEEE J. Quantum Electron.*, vol. 40, no. 11, pp. 1622-1628, Nov. 2004.

[24] M. Yañez and J. C. Cartledge,"Extraction of intrinsic and extrinsic parameters in electroabsorption modulators," *IEEE Trans. Microw. Theory Tech.* vol. 58, no. 8, pp. 2284-2291, Aug. 2010.

[25] P. J. Steven, M. Whitehead, G. Parry, K. Woodbridge, "Computer modeling of the electric field dependent absorption spectrum of multiple quantum well material," *IEEE J. Quantum Electron*., vol. 24, no. 10, pp. 2007-2016, Oct. 1988.

[26] X. Wang, S. Yu,, J. Qin, A. C. Covian, H. Zuo, X. Sun, J. Hu, T. Gu, and J. Liu, "Low-voltage, coupled multiple quantum well electroreflective modulators towards ultralow power inter-chip optical interconnects," *J. Lightw. Technol*, vol. 38, no. 13, pp. 3414-3421, July 2020.